Effects of *N*-heteroaromatic ligands on highly luminescent mononuclear copper(I)-halide complexes

Hiroki Ohara,[a] Atsushi Kobayashi,[a, b] Masako Kato[a]*

[a] Department of Chemistry, Faculty of Science, Hokkaido University, North-10 West-8, Kita-ku, Sapporo, Hokkaido 060-0810, Japan

[b] Precursory Research for Embryonic Science and Technology (PRESTO), Japan Science and Technology Agency (JST), Honcho 4-1-8, Kawaguchi, Saitama 332-0012, Japan.

Masako Kato, TEL +81-11-706-3817, FAX +81-11-706-3447, mkato@sci.hokudai.ac.jp

ABSTRACT: A series of mononuclear Cu(I)-halide complexes, $[CuX(PPh_3)_2(L)]$ ($X = Cl^-, Br^-, I^-$; PPh_3 = triphenylphosphine; L = pyridine (py), isoquinoline (iq), 1,6-naphthyridine (nap)), were synthesized. The emission color of $[CuX(PPh_3)_2(L)]$ varies from blue to red by changing the L ligands and the halide ions, and all the complexes exhibit high emission quantum yields (0.16-0.99) in the crystals. The emission studies revealed that the emissive states of $[CuX(PPh_3)_2(L)]$ differ depending on the L ligand. Complexes $[CuX(PPh_3)_2(py)]$ and $[CuX(PPh_3)_2(nap)]$ mainly emit from

the singlet metal-to-ligand charge transfer mixed with the halide-to-ligand charge transfer (^{1}(M+X)LCT) state at room temperature. In contrast, emissions from [CuX(PPh_3)$_2$(iq)] at room temperature originate from both ^{3}(M+X)LCT and $^3\pi\pi^*$ states. These results indicate that *N*-heteroaromatic ligands play an important role in the emission properties of mononuclear Cu(I)-halide complexes.

1. Introduction

Luminescent Cu(I) complexes have attracted increasing attention recently as alternative candidates for photofunctional noble metal complexes such as photosensitizers for solar energy conversion [1, 2], luminescence-based sensor materials [3, 4], luminescent materials for organic light-emitting diodes [5-8], and luminescent probes of biological systems [9] because they are highly-efficient and inexpensive. In addition, the characteristic emission properties of 3d metal complexes are also interesting. For example, highly luminescent Cu(I) complexes often exhibit thermally activated delayed fluorescence (TADF) from the singlet metal-to-ligand charge transfer (^{1}MLCT) state to the corresponding triplet state (^{3}MLCT) when the singlet-triplet energy difference is small (around 1000 cm^{-1}) [10, 11]. Previously, Yersin *et al*. reported that Cu(I) complexes such as [Cu(POP)(NN)] (POP = bis[2-(diphenylphosphino)phenyl]ether, NN = bidentate pyrazolylborate) were efficient TADF emitters for use in OLEDs [12]. The triplet state of Cu(I) complexes can have longer lifetimes than

those of noble metal complexes because of the reduced mixing of singlet components resulting from their smaller spin-orbit coupling constant. On the other hand, a long lifetime for the stable excited state should be advantageous for photochemical reactions and sensing. In this context, Mann *et al.* reported long-lived $^3\pi\pi^*$ luminescence from $[Cu(isocyanide)_2(dmp)]^+$ (dmp = 2,9-dimethyl-1,10-phenanthroline) in crystals for oxygen gas sensing [4]. These complexes exhibit almost millisecond emission lifetimes, and are efficient dioxygen sensors. Therefore, Cu(I) complexes exhibit versatile properties necessary for photofunctional materials.

Recently, we found that mononuclear Cu(I)-halide complexes, $[CuX(PPh_3)_2(L)]$ (X = halide ion, PPh_3 = triphenylphosphine, L = *N*-heteroaromatic ligands) exhibit extremely intense luminescence in spite of their simple structures [13, 14]: Complexes bearing a 4-methylpyridine (4-Mepy), $[CuX(PPh_3)_2(4\text{-Mepy})]$, show a strong blue emission derived from the ^{1}MLCT state combined with the singlet halide-to-ligand charge transfer (^{1}XLCT) state (*i.e.* ^{1}(M+X)LCT) at room temperature. We also reported that the mononuclear complexes can be prepared by simply grinding the materials. Furthermore, changing the *N*-heteroaromatic ligands (L) on the strongly luminescent Cu(I)-iodide complexes $[CuI(PPh_3)_2(L)]$ (L = pyridine (py), 1,6-naphthyridine (nap), or isoquinoline (iq)) changed the emission wavelength from blue-green to yellow [14]. Although the effect of *N*-heteroaromatic ligands (L) on the emission wavelength of Cu(I)-halide complexes is well known [15-17], investigations regarding the origin of significant changes in the emission wavelengths have

not been described in detail.

In this paper, we aim to understand the effect of *N*-heteroaromatic ligands on the emission properties of the mononuclear Cu(I)-halide complexes by systematically preparing a series of complexes [CuX(PPh_3)$_2$(L)] (Scheme 1; X = Cl^-, Br^-, or I^-; L = py (**1-X**), iq (**2-X**), or nap (**3-X**)) and investigating their photoluminescence properties in detail. To this end, we prepared complexes that are colorful strong emitters with high quantum yields (0.16–0.99), and with emission colors that changed from blue to red depending on the combination of *N*-heteroaromatic ligand and halide ion.

2. Experimental

2.1. *Materials and synthesis*

All copper(I) halides, ligands, and solvents available commercially were used as received without further purification. Unless otherwise stated, all manipulations were conducted in air. The Cu(I) complexes [CuCl(PPh_3)$_3$]·CH_3CN [18], [CuBr(PPh_3)$_3$] [19], [CuI(PPh_3)$_3$] [20] were prepared according to the reported procedures. [CuX(PPh_3)$_2$(py)] (**1-X**, X = Cl^-, Br^-, or I^-) were prepared in the same way and confirmed crystallographically to have the same crystal structures as those reported previously [21]. Synthetic procedures for **3-I** are described in our previous report [14]. Although the preparation of [CuI(PPh_3)$_2$(iq)] (**2-I**) is also reported in our previous study [14], we found that polymorphic crystals are produced depending on the amount of PPh_3 added (see *Crystal*

structures section), which are named as **2-I-α** and **2-I-β**. The preparation of **2-I-β** is described below.

[CuCl(PPh$_3$)$_2$(iq)] (**2-Cl**). To [CuCl(PPh$_3$)$_3$]·CH$_3$CN (90.4 mg, 0.098 mmol) was added iq (1 mL) and the yellow precipitate was formed. CHCl$_3$ (1 mL) was added to the mixture to dissolve the precipitate. The title compound was obtained as yellow crystals (43.8 mg, 60%) by slow diffusion of diethyl ether vapor into the copper solution for 18 h. Elemental analysis calculated for $C_{45}H_{37}CuClNP_2$: C 71.80, H 4.95, N 1.86; found C 71.86, H 4.74, N 1.91. ^{1}H NMR (270 MHz, $CDCl_3$) δ ppm 7.19 - 7.44 (m, 30 H) 7.56 - 7.78 (m, 3 H) 7.82 (d, J = 8.2 Hz, 1 H) 7.94 (d, J = 8.2 Hz, 1 H) 8.53 (s, 1 H) 9.27 (s, 1 H).

[CuBr(PPh$_3$)$_2$(iq)] (**2-Br**). To a suspension of CuBr (37.5 mg, 0.24 mmol) in iq (1 mL) was added PPh$_3$ (153.8 mg, 0.59 mmol) and the yellow precipitate was formed. CHCl$_3$ (2 mL) was added to the mixture to dissolve the precipitate, and then filtered to remove the green impurity. The title compound was obtained as yellow crystals (128.7 mg, 69%) by slow diffusion of diethyl ether vapor into the copper solution for 14 h. Elemental analysis calculated for $C_{45}H_{37}CuBrNP_2$: C 67.80, H 4.68, N 1.76; found C 67.66, H 4.49, N 1.78. ^{1}H NMR (270 MHz, $CDCl_3$) δ ppm 7.15 - 7.45 (m, 30 H) 7.57 - 7.75 (m, 3 H) 7.83 (d, J = 7.9 Hz, 1 H) 7.94 (d, J = 7.6 Hz, 1 H) 8.52 (d, J = 5.6 Hz, 1 H) 9.27 (s, 1 H).

[CuI(PPh$_3$)$_2$(iq)] (**2-I-β**). To a suspension of CuI (48.9 mg, 0.26 mmol) in iq (1 mL) was added PPh$_3$ (660 mg, 2.5 mmol) and the yellow precipitate was formed. CHCl$_3$ (1 mL) was added to the mixture

to dissolve the precipitate. The title compound was obtained as yellow crystals (177.1 mg, 85%) by slow diffusion of diethyl ether vapor into the copper solution for 10 h. Elemental analysis calculated for $C_{45}H_{37}CuINP_2$: C 64.02, H 4.42, N 1.66; found C 64.28, H 4.23, N 1.68. ^{1}H NMR (270 MHz, $CDCl_3$) δ ppm 7.06 - 7.49 (m, 30 H) 7.58 - 7.76 (m, 3 H) 7.83 (d, J = 8.2 Hz, 1 H) 7.96 (d, J = 8.2 Hz, 1 H) 8.54 (d, J = 5.9 Hz, 1 H) 9.27 (s, 1 H).

[CuCl(PPh$_3$)$_2$(nap)] (**3-Cl**) (nap = 1,6-naphthyridine). $[CuCl(PPh_3)_3]\cdot CH_3CN$ (49.6 mg, 0.054 mmol) was dissolved in a $CHCl_3$ solution (1 mL) of nap (100 mg, 0.77 mmol). The title compound was obtained as yellow crystals (20.5 mg, 52%) by slow diffusion of diethyl ether vapor into the copper solution for 3 d. Elemental analysis calculated for $C_{44}H_{36}CuClN_2P_2$: C 70.12, H 4.81, N 3.72; found C 70.17, H 4.67, N 3.76. ^{1}H NMR (270 MHz, $CDCl_3$) δ ppm 7.20 - 7.43 (m, 30 H) 7.56 (dd, J = 8.2, 4.3 Hz, 1 H) 7.93 (d, J = 5.9 Hz, 1 H) 8.26 - 8.37 (m, 1 H) 8.75 (d, J = 5.9 Hz, 1 H) 9.13 (dd, J = 4.3, 2.0 Hz, 1 H) 9.32 (s, 1 H).

[CuBr(PPh$_3$)$_2$(nap)] (**3-Br**). $[CuBr(PPh_3)_3]$ (56.8 mg, 0.061 mmol) was dissolved in a $CHCl_3$ solution (1 mL) of nap (100 mg, 0.77 mmol). The title compound was obtained as yellow crystals (43.1 mg, 89%) by slow diffusion of diethyl ether vapor into the copper solution for 38 h. Elemental analysis calculated for $C_{44}H_{36}CuBrN_2P_2$: C 66.21, H 4.55, N 3.51; found C 66.10, H 4.47, N 3.48. ^{1}H NMR (270 MHz, $CDCl_3$) δ ppm 7.13 - 7.46 (m, 30 H) 7.56 (dd, J = 8.6, 4.3 Hz, 1 H) 7.92 (d, J = 5.9 Hz, 1 H) 8.25 - 8.36 (m, 1 H) 8.75 (d, J = 5.9 Hz, 1 H) 9.13 (dd, J = 4.3, 2.0 Hz, 1 H) 9.32 (s, 1 H).

2.2. *Luminescence measurements*

The luminescence spectrum of each sample was measured using a JASCO FR-6600 spectrofluorometer at room temperature. The luminescence quantum yield was recorded on a Hamamatsu Photonics C9920-02 absolute photoluminescence quantum yield measurement system equipped with an integrating sphere apparatus and 150-W CW xenon light source. An A10095-03 non-luminescent quartz sample holder (Hamamatsu Photonics) was used for the absolute photoluminescence quantum yield measurement in air. The accuracy of the instrument was confirmed by the measurement of the quantum yield of anthracene in ethanol solution (0.27) [22]. Emission lifetime measurements were conducted by using a Hamamatsu Photonics C4334 system equipped with a streak camera as a photo detector and a nitrogen laser as an excitation light source (λ_{ex} = 337 nm). A liquid N_2 cryostat (Optistat-DN optical Dewar and ITC-503 temperature controller, Oxford Instruments) was used to control the sample temperature.

The emission decays were analyzed using two exponentials, i.e., $I = A_1\exp(-t/\tau_1) + A_2\exp(-t/\tau_2)$, where τ_1 and τ_2 are the lifetimes, and A_1 and A_2 are the pre-exponential factors. For the determination of the radiative and non-radiative rate constants, we used the averaged lifetimes (τ_{av}), which were estimated based on equation (1) for the two exponential decay components [23]:

$$\tau_{av} = \frac{A_1\tau_1^2 + A_2\tau_2^2}{A_1\tau_1 + A_2\tau_2} \qquad (1)$$

2.3. *Single-crystal X-ray diffraction measurements*

All single-crystal X-ray diffraction measurements were conducted using a Rigaku Mercury CCD diffractometer with graphite monochromated Mo Kα radiation (λ = 0.71069 Å) and a rotating anode generator. Each single-crystal was mounted on a MicroMount using paraffin oil. The crystal was then cooled using a N_2-flow type temperature controller. Diffraction data were collected and processed using the CrystalClear software [24]. Structures were solved by the direct method using SIR-2004 [25]. Structural refinements were conducted by the full-matrix least-squares method using SHELXL-97 [26]. Non-hydrogen atoms were refined anisotropically, and hydrogen atoms were refined using the riding model. All calculations were conducted using the Crystal Structure crystallographic software package [27]. Crystallographic data obtained for each complex are summarized in Table 1.

2.4. *Characterization measurements*

The ^{1}H NMR spectrum of each sample was measured using a JEOL EX-270 NMR spectrometer at room temperature. Elemental analysis was conducted at the analysis center at Hokkaido University.

2.5. *Theoretical calculations*

DFT calculations were performed with the B3LYP functional [28, 29] and the LANL2DZ basis [30-31] set using Gaussian 03 [32] for **1-Cl**, **1-Br**, **2-Cl**, **2-Br**, **2-I-β**, **3-Cl**, and **3-Br**. As for the calculations of **1-I**, **2-I-α**, and **3-I**, we have already reported the results using the same functional

and basis set [14]. The atomic coordinates determined for the individual molecular structures by X-ray crystallographic analysis were used for the DFT calculations. The drawing of molecular orbitals for the complexes were made using Avogadro 1.10 [33].

3. Results and discussion

3.1. *Crystal structures*

Figures 1 and 2 show the molecular structures of **2-X** and **3-X** (X = Cl^-, Br^-, I^-), respectively. Crystal structures of **1-X** prepared herein were identical to those reported by Engelhardt *et al.* [21]. All complexes adopt a tetrahedral coordination geometry occupied by one halide, one N atom of the *N*-heteroaromatic ligand, and two P atoms of the PPh_3 ligands. Selected bond lengths and angles around the copper(I) atom of **2-X** and **3-X** are listed in Table 2. For complex **2-I**, two polymorphic crystal structures (**2-I-α** and **2-I-β**) were obtained. Structure **2-I-α** was crystallized from the isoquinoline/chloroform solution including a 1:2 ratio of CuI and PPh_3 [14], while **2-I-β** was obtained from the isoquinoline/chloroform solution including 1:10 ratio of CuI and PPh_3. The important difference between the polymorphic forms of **2-I-α** and **2-I-β** is the cell volume. The volume of **2-I-α** (3864(2) $Å^3$) is larger by about 100 $Å^3$ than that of **2-I-β** (3771.2(7) $Å^3$) in spite of both polymorphs having the same chemical formula. The larger cell volume of **2-I-α**, with a loosely packed structure, is expected to allow structural relaxation in the excited state more effectively than

2-I-*β* (see 3.2.2.). There can be seen another notable difference between the conformation of the iq ligand for **2-Cl** and the other complexes **2-X** (X = Br^- and I^-). The C37 carbon atoms at 3-position of iq are oriented in the direction of the halide anion for **2-Br** and **2-I**, while **2-Cl** adopts an inverted orientation, which is probably a steric effect of the larger halides of **2-Br** and **2-I**. Interestingly, the complexes of **3-X**, **2-Br**, and **2-I-*β*** were found to be isomorphous to each other. Although **3-Cl** has a similar molecular structure to **2-Cl**, the crystal structure of **3-Cl** is different from that of **2-Cl**. The Cu-X bond of **3-Cl** is shorter than that of **2-Cl** (2.3330(9) Å for **2-Cl**, 2.312(1) Å for **3-Cl**) and the Cu-N bond of **3-Cl** is longer than that of **2-Cl** (2.091(3) Å for **2-Cl**, 2.125(3) Å for **3-Cl**). The shorter Cu-X and longer Cu-N bonds of **3-Cl** indicate steric repulsion between the Cl ion and nap ligand. Thus, the steric repulsion between the chloride ion and nap ligand likely causes the differences in the crystal structures between **2-Cl** and **3-Cl**.

3.2. *Emission properties*

3.2.1. *Complexes **1-X** (X = Cl^-, Br^-, I^-)*

Figure 3 shows the emission spectra of **1-X** at 298 K and 77 K in the crystals, and the photophysical parameters of **1-X** are summarized in Table 3. Complexes **1-X** exhibit blue-green light emissions when they are excited with UV light, and the emission maxima at 298 K were observed at 498, 483, and 485 nm for **1-Cl**, **1-Br**, and **1-I**, respectively. All spectra of **1-X** at both 298 and 77 K are broad without vibronic progressions, indicating that the emissive excited states have a

charge-transfer character in this temperature range. Each emission spectrum measured at 77 K shifted to lower energies by ca. 540−850 cm^{-1} than the corresponding spectrum measured at 298 K. Interestingly, the luminescence quantum yields of **1-X** in crystals were found to be extremely high (0.98, 0.95, and 0.99 for **1-Cl**, **1-Br**, and **1-I**, respectively) although the measurements in solution were difficult because of the ligand-dissociation and/or the dimerization as usual for mononuclear Cu(I) complexes [13]. The emission lifetimes of complexes **1-X** in the crystals were estimated to be in the range from several microseconds to several tens of microseconds by least-square fitting of the emission decays (see Experimental). These emission properties of complexes **1-X** are similar to those of $[CuX(PPh_3)_2(4\text{-Mepy})]$ whose emission properties were characterized as delayed fluorescence at room temperature [13]. Therefore, the luminescence of complexes **1-X** could have a similar origin. The different radiative rate constants (k_r) at 298 K and 77 K, k_r values at 298 K are several times larger than that at 77 K, suggest that luminescence of **1-X** may be assigned to delayed fluorescence at room temperature.

To clarify the emission properties in detail, the temperature dependence of the emission lifetimes of complexes **1-X** were investigated. As shown in Figure 4, the lifetimes of complexes **1-X** changed gradually in the low-temperature region. However, a sharp decrease in the lifetime was observed with increasing temperature above 170 K. Assuming a two-state model involving the lowest excited singlet state (S_1) and the lowest excited triplet state (T_1), the observed lifetime can be expressed as a

Boltzmann average by using equation (2) [11, 34-36].

$$\tau_{obs} = \frac{3+exp\left(-\frac{\Delta E}{RT}\right)}{3/\tau_{T_1} + 1/\tau_{S_1} exp\left(-\frac{\Delta E}{RT}\right)} \qquad (2)$$

where ΔE is the energy difference between the singlet and triplet states, τ_{S1} and τ_{T1} are the lifetimes of S_1 (fluorescence) and T_1 (phosphorescence) states, R is the ideal gas constant, and T is the absolute temperature. In this two-state model analysis, the average lifetime was used instead of τ_{obs}, i.e., $\tau_{obs} = \tau_{av}$. The corresponding fitting parameters are listed in Table 4. The obtained ΔE values for **1-X** (740–850 cm^{-1}) are roughly consistent with the spectral shifts of ~1000 cm^{-1} between 298 and 77 K, indicating that the two-state model is reasonable for this temperature range. Using fitting parameters, singlet components of luminescence ($I(S_1)/I_{total}$) can be estimated by using equation (3) [35].

$$\frac{I(S_1)}{I_{total}} = 1 - \left(1 + \frac{\Phi_{S1}\tau_{T1}}{3\Phi_{T1}\tau_{S1}} exp\left(-\frac{\Delta E}{RT}\right)\right)^{-1} \qquad (3)$$

where, Φ_{S1} and Φ_{T1} are luminescence quantum yields of the singlet and triplet states. As noted above, the k_r at 298 K and 77 K and lifetime analysis of complexes **1-X** revealed that the emissive states of complexes **1-X** at 298 K are mainly singlet states and those at 77 K are triplet states, therefore we approximate Φ_{S1} and Φ_{T1} by Φ at 298 K and 77 K, respectively. As a result, the estimated singlet components at 298 K are 57, 53, and 80% for **1-Cl**, **1-Br**, and **1-I**, respectively (Table 4). While the emission of **1-I** is mainly from the singlet state at 298 K, the singlet components of emission from **1-Cl** and **1-Br** are no more than 60%. The smaller singlet emission components would result in the

larger k_r values of **1-Cl** and **1-Br** for the phosphorescence component ($1.9–3.3 \times 10^4$ s^{-1}) compared to that of **1-I** (1.1×10^4 s^{-1}) because ΔE values are comparable to each other. Taking account of the heavy atom effect, the k_r values of **1-X** at 77 K are expected to increase in the following order **1-Cl** < **1-Br** < **1-I**. However, the obtained results showed the opposite trend. It is noteworthy that the trend can be seen also in the 4-Mepy complexes, $[CuX(PPh_3)_2(4\text{-Mepy})]$ [13] and **3-X** (*vide infra*) which have the ^{1,3}(M+X)LCT emission state, while the **2-X** complexes with the $^3\pi\pi^*$ emission state exhibit a normal trend of the halide effect (*vide infra*). Further investigation concerning the properties of the triplet sublevels would be necessary for the elucidation of the halide effects on the (M+X)LCT emission state.

3.2.2. *Complexes **2-X** ($X = Cl^-, Br^-, I^-$)*

Figure 5 shows the emission spectra of **2-X** at 298 K and 77 K in the crystals. In contrast to the spectra of **1-X**, those of **2-X** exhibit vibronic structures except for those of **2-Cl** and **2-I-β** at 298 K, which suggests $^3\pi\pi^*$ character of the luminescence. The longer lifetimes (300–1300 μs at 77 K) for **2-X** compared to those found for **1-X** support this assignment. The order of k_r at 77 K ([4.4, 3.6, 9.5, and 16]$\times 10^2$ s^{-1} for **2-Cl**, **2-Br**, **2-I-β**, **2-I-α**, respectively) show a normal trend of the heavy atom effect of the halide ions. Furthermore, complexes **2-Cl** and **2-I-β** exhibit rather long lifetimes even at room temperature (506 and 376 μs, respectively), which is consistent with the spectral profiles of the vibronic structures. On the other hand, the broad spectra of **2-Br** and **2-I-α** can be assigned to

emission from the triplet CT state because of their shorter lifetimes (132 and 65 μs, respectively) compared to those of **2-Cl** and **2-I-*β*** at 298 K. Thus, the complexes **2-X** bearing an isoquinoline are interesting systems with competitive emission states between the triplet CT and $^3\pi\pi^*$. It is noteworthy that the two polymorphic forms **2-I-*α*** and **2-I-*β*** provide different emission spectra at 298 K although the structured spectra at 77 K are essentially the same. As discussed in the *crystal structures* section, the cell volume of **2-I-*α*** is ca. 100 $Å^3$ larger than that of **2-I-*β***, which suggests that structural relaxation could occur more effectively in the excited state. Structural relaxation in the excited state probably stabilizes the CT excited state more effectively than the ππ* state, because the MLCT excited state for tetrahedral Cu(I) complexes is liable to flattening distortion resulting in the broad emission spectrum observed for **2-I-*α*** at 298 K. The emission wavelength of **2-Br** is longer than that of **2-I**, indicating that the emission energy depends on the halide anion as observed for the charge-transfer type emissions of halide-bridged dinuclear complexes [15]. Therefore, the CT excited state of **2-Br** is more stabilized than the excited state of **2-I**, which results in the broad emission spectrum of **2-Br**. In addition, **1-X** and **2-X** also exhibit relatively high luminescence quantum yields (0.44–0.73) at 298 K; however, the values decreased to 0.20–0.51 at 77 K. The reverse trend in the quantum yields supports the contribution to the emission from different emission states (i.e. $^3\pi\pi^*$ and ^{3}(M+X)LCT) at 298 K, although the emission occurs from only $^3\pi\pi^*$ state at 77 K.

3.2.3. *Complexes* ***3-X*** *(X = Cl^-, Br^-, I^-)*

Figure 6 shows the emission spectra of **3-X** at 298 K and 77 K in the crystals. The spectral profiles of **3-X** are similar to those of **1-X**, suggesting that the emission occurs from the triplet CT state, although the emission maxima appear at much longer wavelengths (571, 608, and 636 nm for **3-I**, **3-Br**, and **3-Cl**, respectively). In contrast to **1-X** and **2-X**, the emission wavelengths of **3-X** clearly show the halide-ligand dependence. The order of the emission wavelengths is consistent with the increasing ligand field strength of the halide ion in the complexes ($I^- < Br^- < Cl^-$). This trend is similar to that observed for the charge-transfer type emissions of halide-bridged dinuclear complexes [8, 17, 35]. Lower energy shifts (420−890 cm^{-1}) in the emission spectra at 77 K again suggest the contribution from delayed fluorescence at 298 K.

One additional characteristic found for **3-X** is the trend of the emission quantum yield decreases drastically in the order of **3-I**, **3-Br**, and **3-Cl** (0.77, 0.44, and 0.16, respectively), which may be explained by the energy gap law [37, 38]. As shown in Figure 7, the plots of $\ln(k_{nr})$ vs. wavenumber at the emission maxima roughly exhibit a linear relation. The decrease in emission quantum efficiency with decreasing emission energy is interesting since competing nonradiative processes become more relevant (*vide infra*). The lower luminescence quantum yields at 77 K (0.08 for **3-Cl**, 0.25 for **3-Br**, and 0.63 for **3-I**) compared with those at 298 K suggest that the emissive states at room temperature and low temperature are different as in the case of **1-X**.

As shown in Figure 8, a two-state analysis of the temperature dependence of averaged emission lifetime for **3-X** is presented in the same way as that described for **1-X**. The results for **3-X** as well as **1-X** are summarized in Table 4. The ΔE values (550–710 cm^{-1}) for **3-X** are roughly consistent with the spectral shifts of ~1000 cm^{-1} between 298 and 77 K, which indicates the two-state model is reasonable for this temperature region. The luminescent singlet components of **3-X** were estimated to be 93–94% at 298 K by using equation (3), which indicates **3-X** emit mainly from the singlet state at room temperature.

3.4. *Luminescence mechanism*

Scheme 2 shows the schematic energy level diagram of complexes **1-X**–**3-X**. For **1-X**, the ^{1}(M+X)LCT state is easily thermally accessible from the ^{3}(M+X)LCT emissive state at room temperature because the ΔE between these states is small. However, the luminescent singlet components of **1-X** are only 53-80%. This is probably due to the large phosphorescent rate constant of **1-X**, thus the delayed fluorescent process competes with the phosphorescent process. Therefore, **1-X** emits light from both the ^{1}(M+X)LCT and ^{3}(M+X)LCT state at room temperature. At low temperatures, on the other hand, complexes **1-X** emit phosphorescence from the ^{3}(M+X)LCT state because the thermally activation to ^{1}(M+X)LCT state is suppressed. Complexes **3-X** also exhibit similar emission behavior and the luminescent singlet components of **3-X** are almost 100%. Therefore, complexes **3-X** mainly emit delayed fluorescence from the ^{1}(M+X)LCT state at room

temperature. In contrast to **1-X** and **3-X**, the origins of the emission of **2-X** are different. The emission studies clearly indicate the involvement of the $^3\pi\pi^*$ state in the emission states of **2-X**, although the TD-DFT calculations corresponding to the light absorption process suggest that the lowest singlet excited states are all the (M+X)LCT state, including those of **2-X** (see Supporting Information). It is interesting to note that the $\pi\pi^*$ (L) transition energies of **1-I**–**3-I** (HOMO-20 to LUMO, HOMO-5 to LUMO, and HOMO-13 to LUMO for **1-I**, **2-I**, and **3-I**, respectively) are different from each other (6.512, 4.804, and 4.900 eV for **1-I**, **2-I**, and **3-I**, respectively). Thus the $\pi\pi^*$(L) transition energies are relatively small for **2-X**, which are consistent with those of the free ligand L [39-42]. The small energy difference for **2-I** suggests that the (M+X)LCT state and the $\pi\pi^*$ state of **2-I** are more accessible to each other than those of **1-I** and **3-I**. Experimentally the phosphorescence maximum of the iq ligand is observed at 520 nm [41, 42] and the emission maxima of **2-I** is 520–530 nm, which proves that the ^{3}(M+X)LCT and $^3\pi\pi^*$ states of **2-I** should be close in energy and can be thermally accessible to each other, although the $^3\pi\pi^*$ levels of **1-I** and **3-I** are much higher than the ^{3}(M+X)LCT levels. The characteristic properties of **2-I** appeared as the different emission spectra between the two morphs of **2-I** (α and β) at room temperature. The difference in the flexibility between them in the crystal could give rise to the different spectral features as discussed in section 3.2.2; more flexible **2-I-**α can be relaxed structurally forming more stabilized ^{3}(M+X)LCT state.

4. Conclusion

The luminescent properties of mononuclear copper(I)-halide complexes with a *N*-heteroaromatic ligand, $[CuX(PPh_3)_2(L)]$ ($X = Cl^-$, Br^-, I^-; L = py, iq, nap), were investigated in detail. All of the synthesized complexes exhibit high luminescence quantum yields (0.16–0.99), and the emission color varies from red to blue by changing L and the halide ligands. Our emission studies including lifetime analysis revealed that the emissions of complexes **1-X** occur from both the singlet and triplet (M+X)LCT states, and those of complexes **3-X** occur mainly from the singlet state at room temperature. In contrast to **1-X** and **3-X**, emissions of complexes **2-X** occur from both the $^3\pi\pi^*$ excited state and the ^{3}(M+X)LCT state at 298 K. At 77 K, the emissions of complexes **2-X** occur from only the $^3\pi\pi^*$ ligand excited states because repopulation of ^{3}(M+X)LCT from the $^3\pi\pi^*$ ligand excited states are suppressed. This study elucidated that the mononuclear Cu(I) complexes with the ternary ligand system provide simple but highly luminescent materials which can easily change the emission color by the choice of halide and *N*-heteroaromatic ligands. Further studies concerning functionalities of these complexes are in progress.

Supporting Information

Details of DFT calculations for **1-Cl**, **1-Br**, **2-Cl**, **2-Br**, **2-I-*β***, **3-Cl**, and **3-Br**.

CCDC-1034595–1034599 contain the supplementary crystallographic data for **2-Cl**, **2-Br**, **2-I(β)**, **3-Cl**, and **3-Br**, respectively. These data can be obtained free of charge from the Cambridge Crystallographic Data Centre.

Acknowledgements

This work was partially supported by Grants-in-Aid for Scientific Research (B) (23350025), Artificial Photosynthesis (No. 2406), Young Scientists (B) (24750049) from the Ministry of Education, Culture, Sports, Science and Technology (MEXT), Japan.

References

[1] S.P. Luo, E. Mejia, A. Friedrich, A. Pazidis, H. Junge, A.E. Surkus, R. Jackstell, S. Denurra, S. Gladiali, S. Lochbrunner, M. Beller, Angew. Chem. Int. Ed., 52 (2013) 419.
[2] R.S. Khnayzer, C.E. McCusker, B.S. Olaiya, F.N. Castellano, J. Am. Chem. Soc., 135 (2013) 14068.
[3] C.S. Smith, C.W. Branham, B.J. Marquardt, K.R. Mann, J. Am. Chem. Soc., 132 (2010) 14079.
[4] C.S. Smith, K.R. Mann, J. Am. Chem. Soc., 134 (2012) 8786.
[5] J.C. Deaton, S.C. Switalski, D.Y. Kondakov, R.H. Young, T.D. Pawlik, D.J. Giesen, S.B. Harkins, A.J. Miller, S.F. Mickenberg, J.C. Peters, J. Am. Chem. Soc., 132 (2010) 9499.
[6] S. Igawa, M. Hashimoto, I. Kawata, M. Yashima, M. Hoshino, M. Osawa, J. Mater. Chem. C, 1 (2013) 542.
[7] M. Hashimoto, S. Igawa, M. Yashima, I. Kawata, M. Hoshino, M. Osawa, J. Am. Chem. Soc., 133 (2011) 10348.
[8] A. Tsuboyama, K. Kuge, M. Furugori, S. Okada, M. Hoshino, K. Ueno, Inorg. Chem., 46 (2007) 1992.
[9] F. Liu, K.A. Meadows, D.R. McMillin, J. Am. Chem. Soc., 115 (1993) 6699.
[10] Z.A. Siddique, Y. Yamamoto, T. Ohno, K. Nozaki, Inorg. Chem., 42 (2003) 6366.

[11] J.R. Kirchhoff, R.E. Gamache, Jr, M.W. Blaskie, A.A. Del Paggio, R.K. Lengel, D.R. McMillin, Inorg. Chem., 22 (1983) 2380.
[12] R. Czerwieniec, J. Yu, H. Yersin, Inorg. Chem., 50 (2011) 8293.
[13] H. Ohara, A. Kobayashi, M. Kato, Dalton Trans., 43 (2014) 17317.
[14] H. Ohara, A. Kobayashi, M. Kato, Chem. Lett., 43 (2014) 1324.
[15] H. Araki, K. Tsuge, Y. Sasaki, S. Ishizaka, N. Kitamura, Inorg. Chem., 44 (2005) 9667.
[16] K. Tsuge, Chem. Lett., 42 (2013) 204.
[17] D.M. Zink, M. Bächle, T. Baumann, M. Nieger, M. Kühn, C. Wang, W. Klopper, U. Monkowius, T. Hofbeck, H. Yersin, S. Bräse, Inorg. Chem., 52 (2013) 2292.
[18] T. Kräuter, B. Neumüller, Polyhedron, 15 (1996) 2851.
[19] P.O. Dunstan, Thermochim. Acta, 437 (2005) 100.
[20] L. Maini, D. Braga, P.P. Mazzeo, B. Ventura, Dalton Trans., 41 (2012) 531.
[21] L.M. Engelhardt, P.C. Healy, J.D. Kildea, A.H. White, Aust. J. Chem., 42 (1989) 895.
[22] W.H. Melhuish, J. Phys. Chem., 65 (1961) 229.
[23] J.R. Lakowicz, Principles of Fluorescence Spectroscopy, 3rd ed., Springer, New York, 2006, pp 141-143.
[24] CrystalClear, Molecular Structure Corporation, Orem, UT, 2001.
[25] SIR2004, M.C. Burla, R. Caliandro, M. Camalli, B. Carrozzini, G.L. Cascarano, L. De Caro, C. Giacovazzo, G. Polidori, R. Spagna, 2005.
[26] G.M. Sheldrick, Acta Crystallogr., Sect. A: Fundam. Crystallogr., 64 (2008) 112.
[27] CrystalStructure 4.0, Rigaku Corporation, Tokyo, Japan, 2000-2010.
[28] A.D. Becke, J. Chem. Phys., 98 (1993) 5648.
[29] C. Lee, W. Yang, R.G. Parr, Phys. Rev. B, 37 (1988) 785.
[30] P.J. Hay, W.R. Wadt, J. Chem. Phys., 82 (1985) 270 and 299.
[31] W.R. Wadt, P.J. Hay, J. Chem. Phys., 82 (1985) 284.
[32] M.J. Frisch, G.W. Trucks, H.B. Schlegel, G.E. Scuseria, M.A. Robb, J.R. Cheeseman, J.A. Montgomery, Jr, T. Vreven, K.N. Kudin, J.C. Burant, J.M. Millam, S.S. Iyenger, J. Tomasi, V. Barone, B. Mennucci, M. Cossi, G. Scalmani, N. Rega, G.A. Petersson, H. Nakatsuji, M. Hada, M. Ehara, K. Toyoda, R. Fukuda, J. Hasegawa, M. Ishida, T. Nakajima, Y. Honda, O. Kitao, H. Nakai, M. Klene, X. Li, J.E. Knox, H.P. Hratchian, J.B. Cross, C. Adamo, J. Jaramillo, R. Gomperts, R.E. Stratmann, O. Yazyev, A.J. Austin, R. Cammi, C. Pomelli, J.W. Ochterski, P.Y. Ayala, K. Morokuma, G.A. Voth, P. Salvador, J.J. Dannenberg, V.G. Zakrzewski, S. Dapprich, A.D. Daniels, M.C. Starain, O. Farkas, D.K. Malick, A.D. Rabuck, K. Raghavachari, J.B. Foresman, J.V. Ortiz, Q. Cui, A.G. Baboul, S. Clifford, J. Cioslowski, B.B. Stefanov, G. Liu, A. Liashenko, P. Piskorz, I. Komaromi, R.L. Martin, D.J. Fox, T. Keith, M.A. Al-Laham, C.Y. Peng, A. Nanayakkara, M. Challacombe, P.M.W. Gill, B. Johnson, W. Chen, M.W. Wong, C. Gonzalez, J.A. Pople, Gaussian 03 (Revision E. 01), Gaussian, Inc., Wallingford, CT, 2004.

[33] M.D. Hanwell, D.E. Curtis, D.C. Lonie, T. Vandermeersch, E. Zurek, G.R. Hutchison, J. Cheminform., 4 (2012) 17.
[34] Q. Zhang, T. Komino, S. Huang, S. Matsunami, K. Goushi, C. Adachi, Adv. Funct. Mater., 22 (2012) 2327.
[35] M.J. Leitl, F.-R. Kuchle, H.A. Mayer, L. Wesemann, H. Yersin, J. Phys. Chem. A, 117 (2013) 11823.
[36] R. Czerwieniec, K. Kowalski, H. Yersin, Dalton Trans., 42 (2013) 9826.
[37] C.T. Cunningham, K.L.H. Cunningham, J.F. Michalec, D.R. McMillin, Inorg. Chem., 38 (1999) 4388.
[38] J.V. Caspar, T.J. Meyer, J. Am. Chem. Soc., 105 (1983) 5583.
[39] G. Fischer, J. Mol. Spectrosc., 49 (1974) 201.
[40] M. Suzuki, M. Fujita, T. Takemura, H. Baba, Bull. Chem. Soc. Jpn., 61 (1988) 3461.
[41] D.W. Abbott, T. Vo-Dinh, Anal. Chem., 57 (1985) 41.
[42] A.M. Alak, T. Vo-Dinh, Anal. Chem., 60 (1988) 596.

Schemes

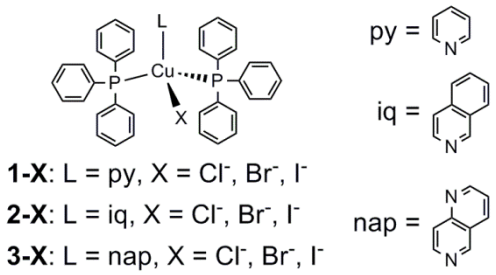

Scheme 1. Structure of $[CuX(PPh_3)_2(L)]$ (X = Cl^-, Br^-, I^-; py = pyridine, iq = isoquinoline, nap = 1,6-naphthyridine).

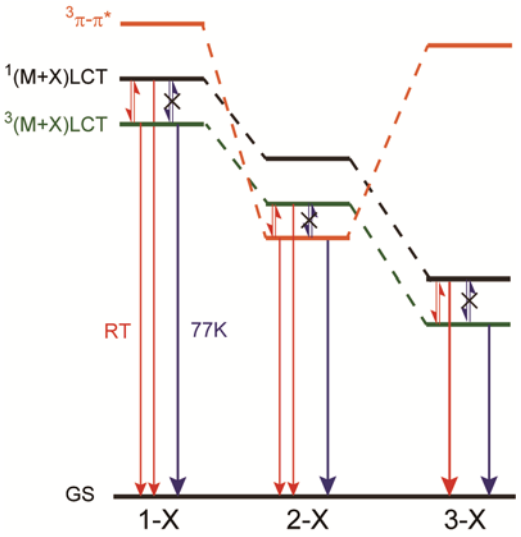

Scheme 2. Schematic energy diagram for the emissive excited states of **1-X**, **2-X**, and **3-X**.

Figures

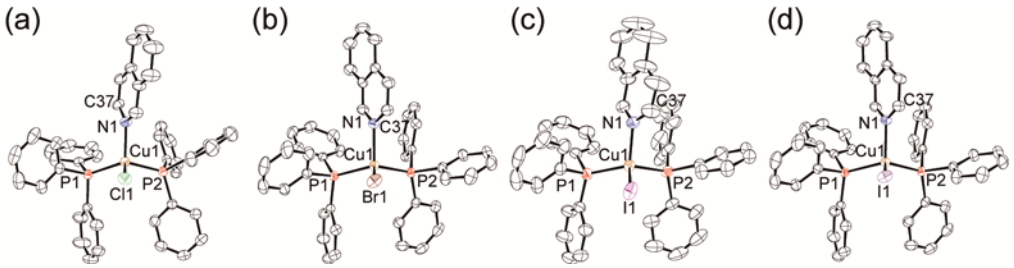

Figure 1. ORTEP drawings of **2-Cl** (a), **2-Br** (b), **2-I-*α*** (c) [14], and **2-I-β** (d). Hydrogen atoms are omitted for clarity. Displacement parameters are drawn at the 50% probability level.

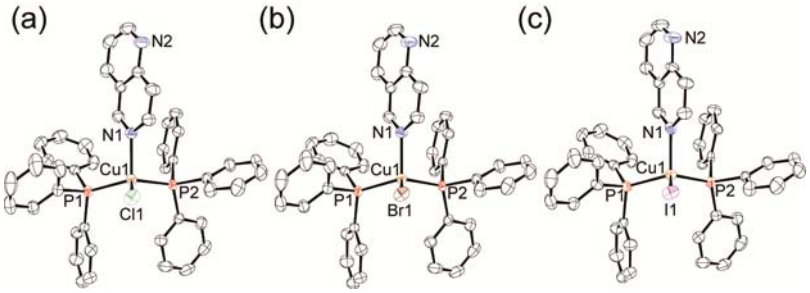

Figure 2. ORTEP drawings of **3-Cl** (a), **3-Br** (b), and **3-I** (c) [14]. Hydrogen atoms are omitted for clarity. Displacement parameters are drawn at the 50% probability level.

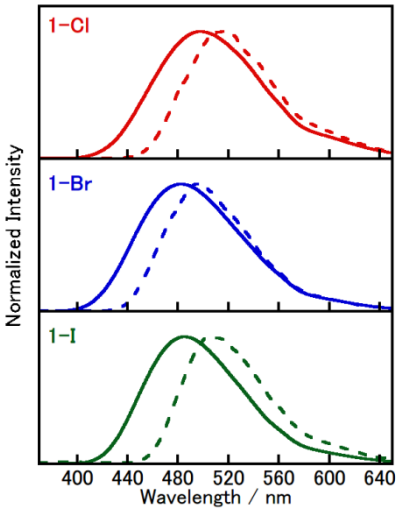

Figure 3. Luminescence spectra of **1-X** in the crystals (λ_{ex} = 350 nm) at 298 K (solid line) and 77 K (dotted line).

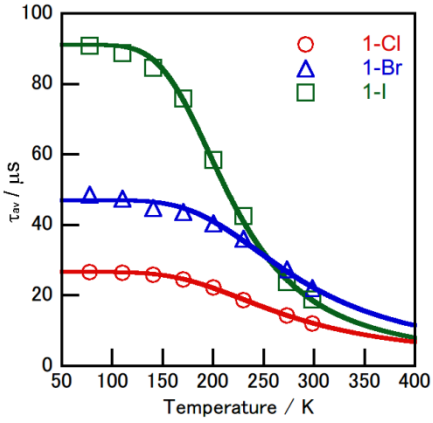

Figure 4. Temperature dependence of the average emission lifetimes of complexes **1-X** in the crystals (λ_{ex} = 337 nm). The solid lines were calculated by using eq. 2.

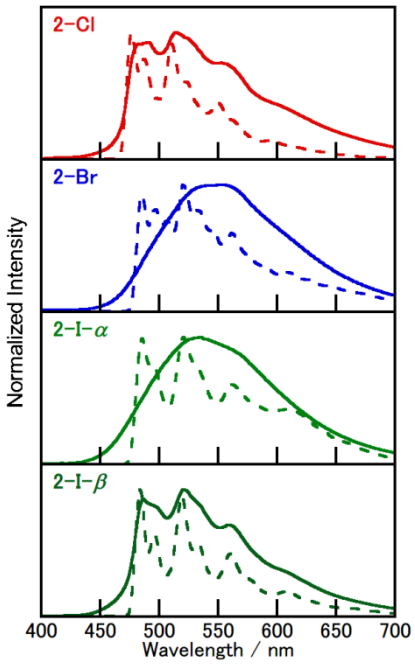

Figure 5. Luminescence spectra of **2-X** in the crystals (λ_{ex} = 370 nm) at 298 K (solid line) and 77 K (dotted line).

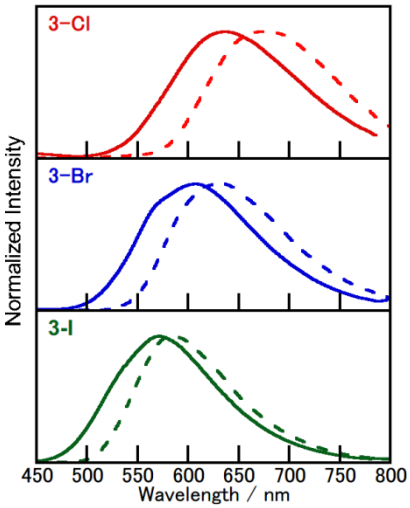

Figure 6. Luminescence spectra of **3-X** in the crystals (λ_{ex} = 400 nm) at 298 K (solid line) and 77 K (dotted line).

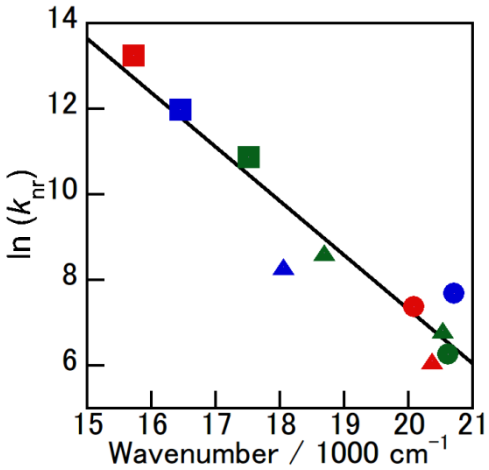

Figure 7. The plots of ln(k_{nr}) vs. wavenumber of **1-X**–**3-X** at the emission maxima; circle: L = py, triangle: L = iq, square: L = nap, red: X = Cl^-, blue: X = Br^-, green: X = I^-.

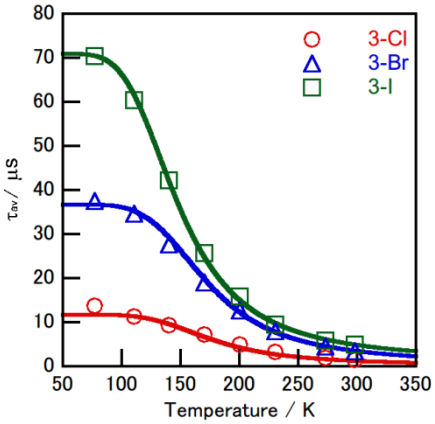

Figure 8. Temperature dependence of the average emission lifetime of complexes **3-X** in the crystals (λ_{ex} = 337 nm). The solid lines were calculated by using eq. 2.

Tables

Table 1. Crystal parameters and refinement data.

	2-Cl	**2-Br**	**2-I-α** [14]	**2-I-β**
T / K	200 (1)	200 (1)	200 (1)	200 (1)
Formula	$C_{45}H_{37}ClCuNP_2$	$C_{45}H_{37}BrCuNP_2$	$C_{45}H_{37}ICuNP_2$	$C_{45}H_{37}ICuNP_2$
Formula weight	752.74	797.19	844.19	844.19
Crystal system	Triclinic	Monoclinic	Monoclinic	Monoclinic
Space group	$P\bar{1}$	$P2_1/n$	$P2_1/c$	$P2_1/n$
a / Å	9.694(3)	9.9964(7)	10.313(3)	10.0363(10)
b / Å	13.320(4)	36.138(2)	18.345(5)	35.870(4)
c / Å	15.401(4)	11.2964(8)	20.464(5)	11.5526(10)
α / °	83.360(9)	90	90	90
β / °	79.997(9)	114.671(2)	93.496(3)	114.936(3)
γ / °	77.599(9)	90	90	90
V / Å^3	1906.4(9)	3708.4(5)	3864.3(16)	3771.2(7)
Z	2	4	4	4
D_{cal} / g cm^{-3}	1.311	1.428	1.296	1.487
Reflections collected	15589	22699	27817	21108
Unique reflections	8633	8252	8328	8416
R_{int}	0.0542	0.0398	0.0450	0.0377
GOF	1.004	1.088	1.109	1.193
R_1 ($I > 2\sigma(I)$)^a	0.0514	0.0422	0.0541	0.0353
wR_2^{b}	0.1271	0.0915	0.1450	0.0944

(Table 1 continued)

	3-Cl	**3-Br**	**3-I** [14]
T/ K	200 (1)	200 (1)	200 (1)
Formula	$C_{44}H_{36}ClCuN_2P_2$	$C_{44}H_{36}BrCuN_2P_2$	$C_{44}H_{36}ICuN_2P_2$
Formula weight	753.73	798.18	845.18
Crystal system	Monoclinic	Monoclinic	Monoclinic
Space group	$P2_1/n$	$P2_1/n$	$P2_1/n$
a / Å	9.8962(8)	9.906(2)	9.9705(7)
b / Å	36.755(2)	36.302(8)	35.823(2)
c / Å	11.1003(10)	11.286(3)	11.5829(7)
α / °	90	90	90
β / °	114.926(4)	114.563(2)	114.770(2)
γ / °	90	90	90
V/ Å^3	3661.5(5)	3691(2)	3756.5(4)
Z	4	4	4
D_{cal} / g cm^{-3}	1.367	1.436	1.494
Reflections collected	39704	22761	23121
Unique reflections	8323	8137	8355
R_{int}	0.0346	0.0304	0.0425
GOF	1.078	1.263	1.193
R_1 ($I > 2\sigma(I)$)[a]	0.0377	0.0396	0.0358
wR_2 [b]	0.0857	0.1049	0.0864

[a] $R_1 = \Sigma||F_o| - |F_c||/\Sigma|F_o|$. [b] $wR_2 = [\Sigma w(F_o^2 - F_c^2)/\Sigma w(F_o)^2]^{1/2}$, $w = [\sigma_c^2(F_o^2) + (xP)^2 + yP]^{-1}$, $P = (F_o^2 - 2F_c^2)/3$.

Table 2. Selected bond distances (Å) and bond angles (°) around copper(I) ions in the complexes **2-X** and **3-X**.

	2-Cl	**2-Br**	**2-I-α** [14]	**2-I-β**
Cu-X	2.3330(9)	2.4546(6)	2.6514(8)	2.6288(5)
Cu-N	2.091(3)	2.1223(18)	2.125(4)	2.120(2)
Cu-P1	2.2493(10)	2.2830(8)	2.2711(13)	2.2858(8)
Cu-P2	2.2671(8)	2.2781(8)	2.2782(14)	2.2807(8)
X-Cu-P1	104.32(3),	104.85(3)	101.50(4)	103.90(3)
X-Cu-P2	106.79(3)	116.11(3)	113.50(4)	116.42(3)
X-Cu-N	99.01(7)	101.78(8)	108.24(10)	101.93(8)
X-Cu-N-C (L)	25.47(17)	34.66(17)	40.2(3)	32.32(17)

	3-Cl	**3-Br**	**3-I** [14]
Cu-X	2.3120(10)	2.4520(8)	2.6307(5)
Cu-N	2.125(3)	2.1226(19)	2.1218(17)
Cu-P1	2.2712(9)	2.2758(9)	2.2819(7)
Cu-P2	2.2709(9)	2.2741(9)	2.2821(8)
X-Cu-P1	105.27(3)	104.27(3)	103.58(3)
X-Cu-P2	115.92(3)	116.33(3)	116.93(3)
X-Cu-N	102.43(6)	102.22(8)	102.14(7)
X-Cu-N-C (L)	40.79(13)	37.27(17)	32.29(16)

Table 3. Luminescence properties of complexes **1-X**, **2-X**, and **3-X** in the crystals at 298 K and 77 K.

compound	**1-Cl**		**1-Br**		**1-I**	
	298K	77K	298K	77K	298K	77K
λ_{max} [a](nm)	498	516	483	496	485 [g]	506
τ (μs (A_n))[b]	3.3 (0.13)	7.5 (0.12)	21.1 (0.84)	40.0 (0.43)	10 (0.21)	28 (0.14)
	12.5 (0.89)	27.4 (0.88)	27.0 (0.14)	53.6 (0.57)	20 (0.82) [g]	94 (0.84)
Φ[f]	0.98	0.89	0.95	0.93	0.99 [g]	0.99
τ_{av} [d](μs)	12	27	22	49	19	91
k_r [e](s^{-1})	8.0×10^4	3.3×10^4	4.3×10^4	1.9×10^4	5.2×10^4	1.1×10^4
k_{nr} [f](s^{-1})	1.6×10^3	4.1×10^3	2.2×10^3	1.4×10^3	5.3×10^2	1.1×10^2

compound	**2-Cl**		**2-Br**		**2-I-α**		**2-I-β**	
	298K	77K	298K	77K	298K	77K	298K	77K
λ_{max} [a](nm)	491, 515,	476, 488,	554	486, 497,	535 [g]	486, 521,	487, 520,	484, 496,
	553	511, 522,		507, 520,		561, 610	558	520, 532,
		549		532, 561				561, 607
τ (μs (A_n))[b]	154 (0.60)	227 (0.49)	73 (0.58)	152 (0.84)	27 (0.54)	123 (0.94)	79 (0.74)	126 (0.86)
	616 (0.48)	1436(0.54)	165 (0.47)	825 (0.23)	78 (0.52) [g]	534 (0.18)	493 (0.30)	777 (0.23)
Φ[f]	0.77	0.56	0.46	0.20	0.63 [g]	0.51	0.65	0.50
τ_{av} [d](μs)	506	1285	132	553	65	310	376	528
k_r [e](s^{-1})	1.5×10^3	4.4×10^2	3.5×10^3	3.6×10^2	9.8×10^3	1.6×10^3	1.7×10^3	9.5×10^2
k_{nr} [f](s^{-1})	4.5×10^2	3.4×10^2	4.1×10^3	1.4×10^3	5.7×10^3	1.6×10^3	9.3×10^2	9.5×10^2

(Table 3 continued)

compound	3-Cl		3-Br		3-I	
	298K	77K	298K	77K	298K	77K
λ_{max} [a](nm)	636	674	608	634	571[g]	585
τ (μs (A_n))[b]	0.32 (0.12)	3.8 (0.20)	1.6 (0.29)	21.9 (0.033)	4.7 (0.87)[g]	46.2 (0.16)
	1.5 (0.91)	14.4 (0.84)	3.6 (1.6)	61.9 (0.97)	6.3 (0.14)	62.7 (0.84)
Φ [c]	0.16	0.08	0.44	0.25	0.73 [g]	0.63
τ_{av} [d](μs)	1.5	14	3.5	38	5.0	73
k_r [e](s^{-1})	1.1×10^5	5.8×10^3	1.2×10^5	6.6×10^3	1.5×10^5	8.9×10^3
k_{nr} [f](s^{-1})	5.7×10^5	6.7×10^4	1.6×10^5	2.0×10^4	5.3×10^4	5.2×10^3

[a] Emission maximum. [b] Emission lifetime. Emission decays were analyzed with two components: $I = A_1\exp(-t/\tau_1) + A_2\exp(-t/\tau_2)$. [c] Photoluminescence quantum yields in the solid states. [d] Average emission lifetimes were determined by using eq 1. [e] Radiative rate constants k_r were estimated by Φ/τ_{av}. [f] Nonradiative rate constants k_{nr} were estimated by $k_r(1 - \Phi)/\Phi$. [g] ref [14]

Table 4. Fitting parameters of **1-X** and **3-X** based on the two-state model (eq. 2), and estimated luminescent singlet components of **1-X** and **3-X** at 298 K.

	1-Cl	**1-Br**	**1-I**	**3-Cl**	**3-Br**	**3-I**
ΔE [a] (cm^{-1})	740	850	810	710	670	550
$\tau(S_1)$ [b] (ns)	203	230	155	18	51	119
$\tau(T_1)$ [b] (μs)	27	47	91	11	37	71
$I(S_1)/I_{total}$ [c] (%)	57	53	80	93	94	94

[a] Energy difference between S_1 and T_1. [b] Lifetime of the S_1 and T_1 states determined by fitting the data using eq. 2 with the averaged emission lifetime. [c] Determined by using eq. 3.